ISSN: 1687-1006 p
ISSN: 2682-3640 e

The Egyptian International Journal of Engineering Sciences and Technology

https://eijest.journals.ekb.eg/

Vol. 50 (2025) 74–84

DOI: 10.21608/eijest.2024.290682.1276

Investigating land cover effect on dark object subtraction model of atmospheric correction

Asmaa M. Elyamany[a*], Sayed A. Mohamed[b], Ibrahim E. Ziedan [a]

[a] *Department of Computer and Systems Engineering, Faculty of Engineering, Zagazig University*
[b] *National Authority for Remote Sensing and Space Science, 23 Jose f Tito, New Nozha Cairo, Egypt*

A R T I C L E I N F O

Article history:

Received 18 May 2024
Received in revised form 28 October 2024
Accepted 28 October 2024
Available online 28 October 2024

Keywords:

Remote Sensing
Atmospheric Correction
Landsat-8
Sentinel-2
DOS
COST
QUAC
Sen2Cor

A B S T R A C T

An efficient and low-cost atmospheric correction technique is becoming more and more necessary as the fields requiring remote sensing imagery grow. Certain techniques rely on measurements taken on-site, while others rely merely on the image; the latter requires less resources and time. For atmospheric correction, one of the most widely used techniques is the Dark Object Subtraction (DOS). In this study, Landsat-8 and Sentinel-2 data are subjected to the DOS and cosine of the solar zenith correction COST algorithm under varying atmospheric circumstances (July and December). Four distinct land cover classes (water, vegetation, desert, and urban) are used to categorize the data. The corrected DOS scenes are compared using both qualitative and quantitative analysis to the Level 2A of each satellite, as well as to the outcomes of QUick Atmospheric Correction (QUAC) in the case of Landsat-8 and Sentinel-2 Correction (Sen2Cor) results. As the Sentinel-2 DOS demonstrates good results in the vegetation and water scene, the results demonstrate the effectiveness of the DOS in the case of Landsat-8 for the vegetation, water, and urban scenes. But because there were no dark objects in the desert environment, the results were unsatisfactory, especially in clear weather for both satellites.

1. Introduction

. Remote sensing is all about acquiring images of the earth by recording the reading of the satellite sensors which is the reflected sun light from the object of interest. This process produces a satellite image that can be used in many fields such as: Geology[1, 2], Oceanography[3], Agriculture[4, 5], Geothermal mapping[6], Environmental monitoring[7, 8] and many others. The reading from these sensors is delivered as a raw image of Digital Number (DN) as in the case of Landsat-8 or as top of atmospheric reflectance as in the case of the Sentinel-2 which doesn't express the true value of the surface reflectance. As the sun light has crossed a long journey from the sun to the object and from the object to the satellite sensor, the energy from the sun light scattered and absorbed by the atmosphere. The atmosphere affects the image in two ways; the first is scattering and the second is absorption[9] . The scattering effect of the atmosphere is reradiating part of the energy to other directions because of the interaction of the radiation with the air molecules causing the energy to scatter to other directions not along the path of the incident radiation[10]. This depends on the shapes, sizes and the materials of the

*Corresponding author. Tel.: *+201013153374*
E-mail address: eng.a.elyamany@gmail.com

air particles and also the sun zenith angle [11]. The absorption is mainly that the energy is being absorbed by the air molecules. Ozone, carbon dioxide, and water vapor are the main constituents that absorb energy depending on the time and the location. This effect depends on the wavelength of the energy[12] . 99% of the ultraviolet (UV) energy is absorbed by ozone [13]. The visible region of the spectrum is not highly affected by absorption of the energy. Water vapor (H2O) and carbon dioxide (CO2) molecules are the two main constituents that affect the absorption of the infrared radiation[13]. Most of the radiation is absorbed in the far infrared region[14]. So to perform the atmospheric correction process there are some factors to be taken into consideration such as position of the sun, temperature, humidity and whether the sky is clear or contains large molecular structure such as fog, smoke or haze. To eliminate these effects an atmospheric correction algorithm is used. Some atmospheric correction algorithms, such as radiative transfer codes (RTC), require in-site measurements at the time the image was taken, while others, such as (DOS), are entirely dependent on the scene, making it simpler and less expensive. The RTC category is based on complex theoretical modeling of the atmospheric absorption and scattering caused by water vapors, aerosols and gases. Information about the atmosphere conditions in the time the image was taken is needed to perform the calculation. Examples of (RTC) are LOWTRAN[15], MODTRAN[16, 17], HITRAN, 5S and 6S[18]. Meanwhile, image-based methods need no in-person or weather data since the correction is completely based on the scene itself. As a result, this method is *less* expensive than the first. Example of algorithms that uses this method are empirical line (EL)[19-21] and (DOS)[22]. In this paper DOS will be demonstrated in details and applied on Landsat-8 and Sentinel-2 data. The DOS algorithm is presented by Chavez in 1988[22]. In 1992 the DOS algorithm was compared with low-altitude aircraft-based measurements and showed acceptable results[23]. Chavez improved DOS in 1996 [24] to include more than just removing the haze effect, but also the zenith angle effect and the Rayleigh effect, as a result of which a new algorithm, DOS2 or COST, was presented. In 2005 Wu used the COST algorithm on QuickBird data and compared it with ground based measurements and it produced acceptable results in the visible bands and bad results in the NIR band [20]. In 2014 DOS was compared with other atmospheric correction algorithms in urban coastal environment which shows that DOS is a good choice for water scenes[21]. In 2015 a study compared DOS to other atmospheric correction algorithms in highly turbid sediment-loaded tropic lake, showed that DOS was overestimating the ground reflectance[25]. In 2016 DOS algorithm was used on Landsat-8 data and found that it made more appropriate spectral pattern in water body, soil and vegetation[26]. In 2016 it was used on Hyperspectral Imager for the Coastal Ocean (HICO) along with FLAASH the result showed that FLAASH produce better result although DOS is easier and doesn't need complex parameters[27]. In 2017 it was used on Sentinel-2 data the result showed that the DOS algorithm easy to use and doesn't have high computational demand[28]. In 2018 it was used on ALOS AVNIR-2 image data the result showed that the DOS algorithm is more effective and efficient than more robust atmospheric correction method[29]. In 2018 it was applied to GaoFen-1 Wild Field Camera (GF-1 WFV1) data under hazy condition which gave fair results[30]. In 2019 DOS applied on the same images from Landsat-8 and Sentinel-2 and the results showed strong correlation between the two images[31].In 2020 three distinct atmospheric correction techniques: two physical techniques (FLAASH and ATCOR) and one image-based technique (DOS) used for estimating Landsat OLI data over arid and semi-arid regions. The results have demonstrated the image-based method DOS1's significant accuracy in reducing the atmospheric effects of the OLI image. The method's results are nearly identical to those of the physical atmospheric correction method and exhibit good conformity with the ground measurements[32]. According to the findings of a study conducted in 2023 on a few atmospheric correction algorithms (6S, FLAASH, DOS, LaSRC, and Sen2Cor), the DOS method achieved the highest producer's accuracy (PA) and user's accuracy (UA), yielding 100% of both[33].

This study aimed to (1) verify the DOS analysis performance of Landsat-8 and Sentinel 2. (2) make a good knowledge of the impact of the DOS on scenes with uniform and unique land cover. (3) Perform a qualitative and quantitative analysis of the DOS results and compare them to level 2A of the same scene, as well as another atmospheric correction algorithm, QUAC in the case of Landsat-8, and Sen2Cor in the case of Sentinel-2. QUAC is A semi empirical algorithm for multi and hyperspectral imagery that perform atmospheric correction based on the information contained within the scene[34, 35].

The structure was organized as follows. Section 2 introduced data and analytical methods. Section 3 analyzed DOS verification, spatiotemporal distributions and, the sensitivities of composed DOS components to Atmospheric variables were further discussed in Section 3. Finally, conclusions were provided in Section 4

2. MATERIALS AND METHOD

2.1. Data Collection

The areas chosen for the experiment are the area of Port Said and Cairo in Egypt. Subsets were taken from scenes in two different dates 3 July, 2019with clear atmosphere and 10 December, 2019 with cloudy atmosphere, and in different land cover characteristics. The first

subset is water with depth not more than 30m, the second is vegetation, the third is desert and the forth is urban. Landsat-8 satellite data with the first 7 bands[36] and Sentinel-2 satellite data with 12 bands[37] were used in this analysis. The original scenes are showed in Figure 1.

Water Vegetation Desert Urban

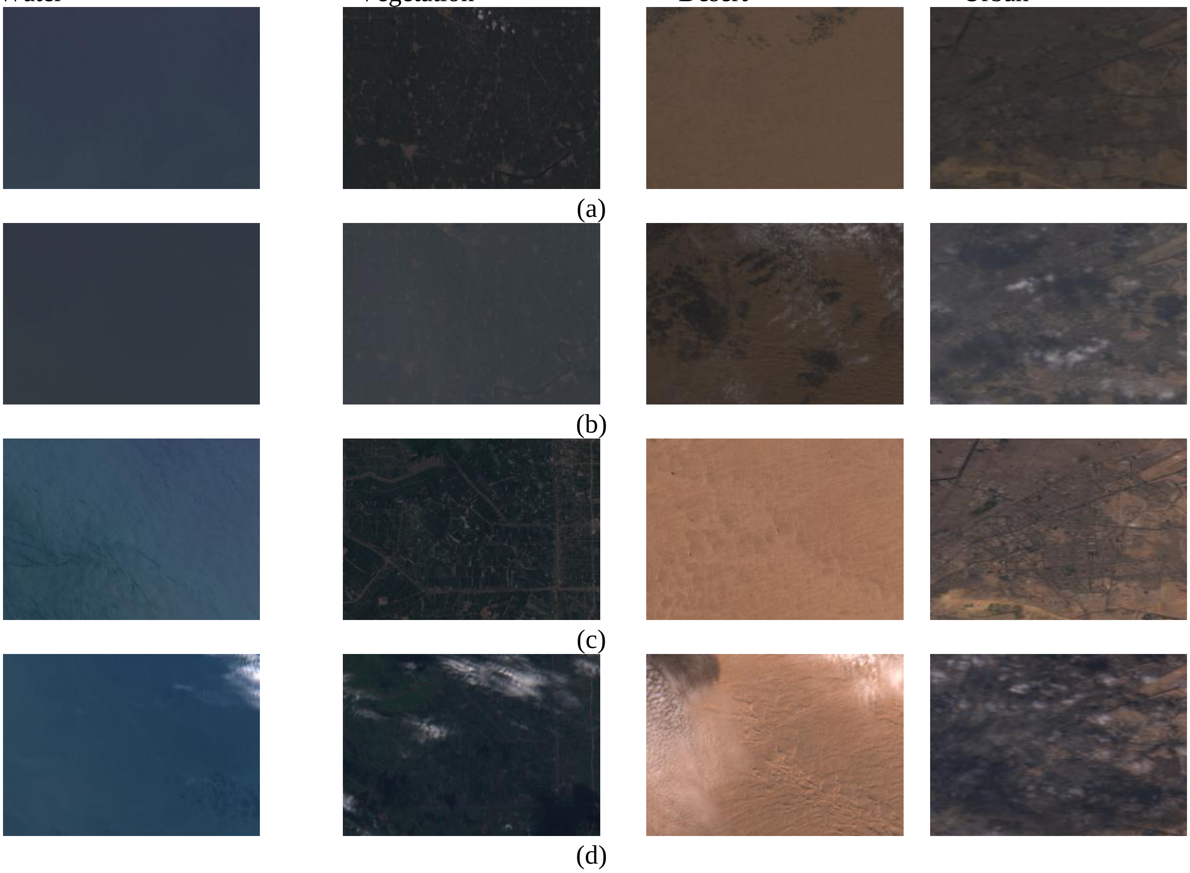

Fig. 1. The original scenes used in the study: (a) Landsat-8 in 3 July 2019; (b) Landsat-8 in 10 December 2019; (c) Sentinel-2 in 3 July 2019; (d) Sentinel-2 in 10 December 2019.

2.2. Dark Object Subtraction (DOS)

The dark object subtraction method in its simplest form involves subtracting a constant value from the entire image assuming a uniform haze distribution all over the scene[[22]. This constant value is derived from the fact that there is a high probability that some pixels in every image are equal to zero, since there are some spots in the scene in complete shadows due to topography or cloud cover; these pixels should be zero, but due to atmospheric scattering, they have values[29], and if this value is subtracted from the entire scene, the haze effect will be removed. In thispaper, the objective is to convert the satellite digital numbers (DN) values to ground reflectance or absolute surface reflectance as follows:

1- Convert the DN to at-satellite radiance which known as the upwelling radiation at top of the atmosphere. This is done by removing the gain and offset caused by the imaging system with the following equation:

$$L_{sat}=(DN-Offset)/Gain \quad (1)$$

Where L_{sat} is the at-satellite radiance, DN is the digital number in the given pixel offset and gain is the offset and gain of the specific band being corrected and can be obtained from the metadata file that comes with the Landsat-8 scene After that.

2- The at-satellite radiance converted to surface reflectance by eliminating the solar and atmospheric effect. The general equation as presented by Moran 1992[23] is:

$$Ref=\frac{\pi(L_{sat}-L_{haze})}{T_{AUV}(E_o\cos(T_Z)T_{AUZ}+E_{down})} \quad (2)$$

Where Ref is spectral reflectance of the surface L_{haze} is Upwelling atmospheric spectral radiance scattered (W m^{-2} sr^{-1} μm^{-1}) i.e. the path radiance. Atmospheric transmittance along the path from the ground to the sensor is referred as T_{AUV}. E_o is Solar spectral irradiance on a surface perpendicular to the sun's rays outside the atmosphere (W m^{-2} μm^{-1}). The angle of incidence of direct solar flux onto the Earth's surface is denoted by T_Z (solar zenith angle, Thetaz). Atmospheric transmittance along the journey from the sun to the ground surface is referred to as T_{AUZ}. . Due to dispersed solar flux in the atmosphere, E_{down} is Downwelling spectral irradiance at the surface (Wm^{-2} μm^{-1}).

From this general model two algorithms are driven by making different simplifying assumptions that are going to eliminate some certain effects.

Assumed parameter of DOS T_{AUV}=1.0, T_{AUZ} =1.0, E_{down}=0.0 and L_{haze} is derived from the image using the dark object algorithm, by this the scene will be corrected for spectral band solar irradiance, the solar zenith angle and also correct the scattering component of the path radiance. In the case of COST, assume parameter is improved by adding term to correct for atmospheric transmittance. T_{AUZ} is approximated by $\cos(\theta_z)$ where θ_z is the solar zenith angle for bands from 1 to 5 and unity for bands 6,7, with T_{AUV}=1.0, E_{down}=0.0 and L_{haze} as DOS

3- The last step of the algorithm is to calculate the L_{haze} value from the scene; this is done by assuming a 1 % minimum reflectance, which is based on the fact that there are very few fully black objects on the planet.

The resulted image goes through a series of analysis procedure to evaluate the algorithm. Frist, compute the Mean Square Error (MSE) by eq. (3) which indicates the average of correctly identified images to the total number of correctly and non-correctly images with the reference input. The following equation provides a formula for calculation of the MSE:

$$MSE=\frac{1}{nm}\sum_{i=n-1}^{0}\sum_{j=m-1}^{0}(E_{ij}-O_{ij})^2 \quad (3)$$

Where n, m is the number of the rows and columns of the image. The resulted image is referred as E while the original is O.

Second, there are spectral curves, which are diagrams of an object's spectral response at different wavelengths of the electromagnetic spectrum.

Finally, the visual inspection of the image.

2.3. proposed Method

The methodology used in the proposed procedure varies depending on the form of initial data, since Landsat-8 data is in DN format, it must first be translated to top of atmospheric radiance, while Sentinel-2 data is already in top of atmospheric reflectance format. The scenes are selected to highlight a specific aspect, such as the water scene, which focuses solely on the water surface and same for the vegetation, desert and urban.

The Landsat-8 data is going through the algorithm from step one and as noticed in Figure 2 the dark DN of the image is calculated and then go through the same as the entire image. The Landsat-8 image is also corrected by QUAC which was performed by ENVI 5.3. The DOS and QUAC results are compared to the level 2A of the same scenes.

As for level 1C of Sentinel-2; it provides an ortho-rectified top-of-atmosphere reflectance image[38]. The sentinel-2 data is processed using the algorithm from step 3 by finding L_{haze} directly and subtracted from the scene. The Sentinel-2 data is also corrected by Sen2Cor algorithm. It’s based on Atmospheric/Topographic Correction algorithm (ATCOR)[28]and built upon lookup tables from a radiance transfer model (LibRadtran)[39] and scene classification. Basically it is a processor that performs atmospheric corrections on Top-of-Atmosphere Level 1C input data for Sentinel-2 to generate bottom of atmosphere or Level 2A product[40]. These results are also compared to the Level 2A of the same scenes.

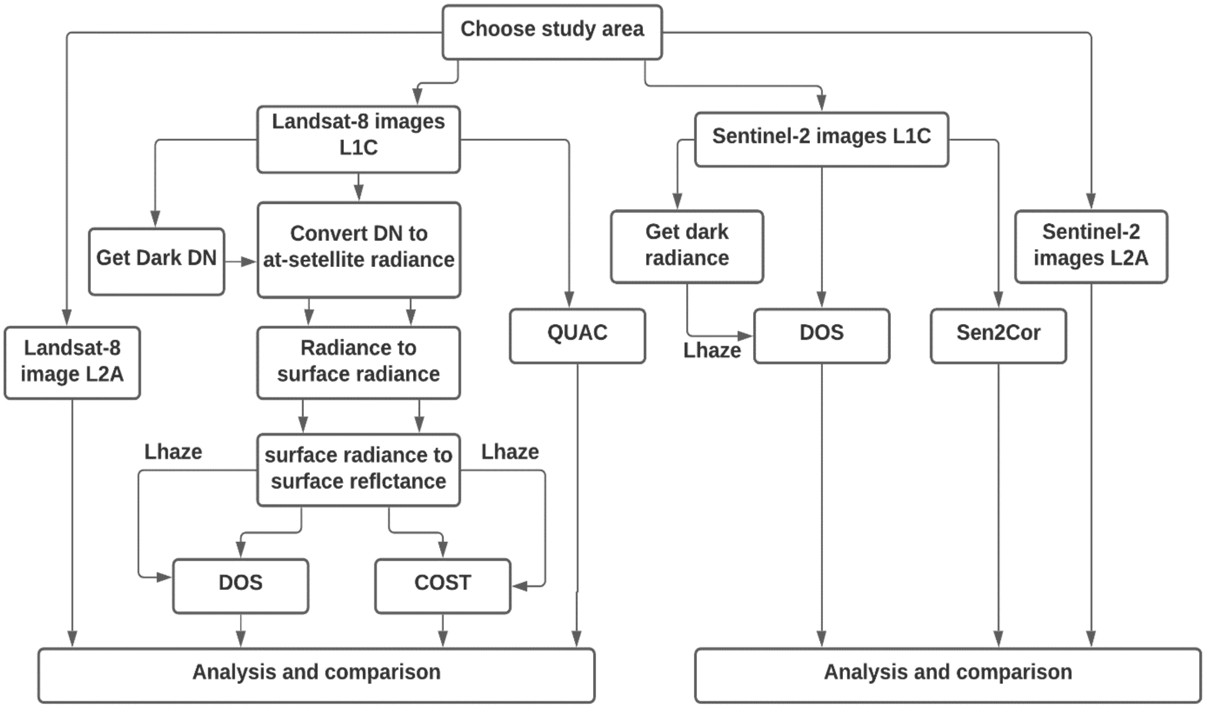

Fig. 2. the proposed workflow

3. Results and Discussion

3.1. The landsat-8 results

From figure 3 the results of DOS and COST are very similar except for the vegetation and urban scene in the hazy weather, the COST beaks around the NIR band. DOS and COST gave error not exceeding 1% except in the desert scenes in both hazy and clear weather conditions while QUAC gave smaller error in the desert scene with clear weather only. From the spectrum curves figure 4 DOS and COST are very close to the Level 2A while the QUAC looks drifting so much far from the level 2A. In the desert scenes it looks that DOS and COST over estimated the error and QUAC is closer to Level 2A in clear weather, the desert scene in clear weather gave a high error as there is no good object can be considered as dark target but on the other hand in the hazy scene the error reduced as the scene contained cloud shadows which considered a good dark target. It is noticed that most of the MSE graphs shows a peak at the NIR that is because in both vegetation and desert reflects high amount of energy in the NIR band that make the scene very bright and the dark target fewer in the other hand the water absorbs a large amount of energy in the NIR band that makes the scene much darker so no beak in the MSE. In figure 5 the visual inspection shows that both DOS and COST keep the details of the image and don't cause distortions but overestimate the error especially in the water scene and clear weather desert scene.

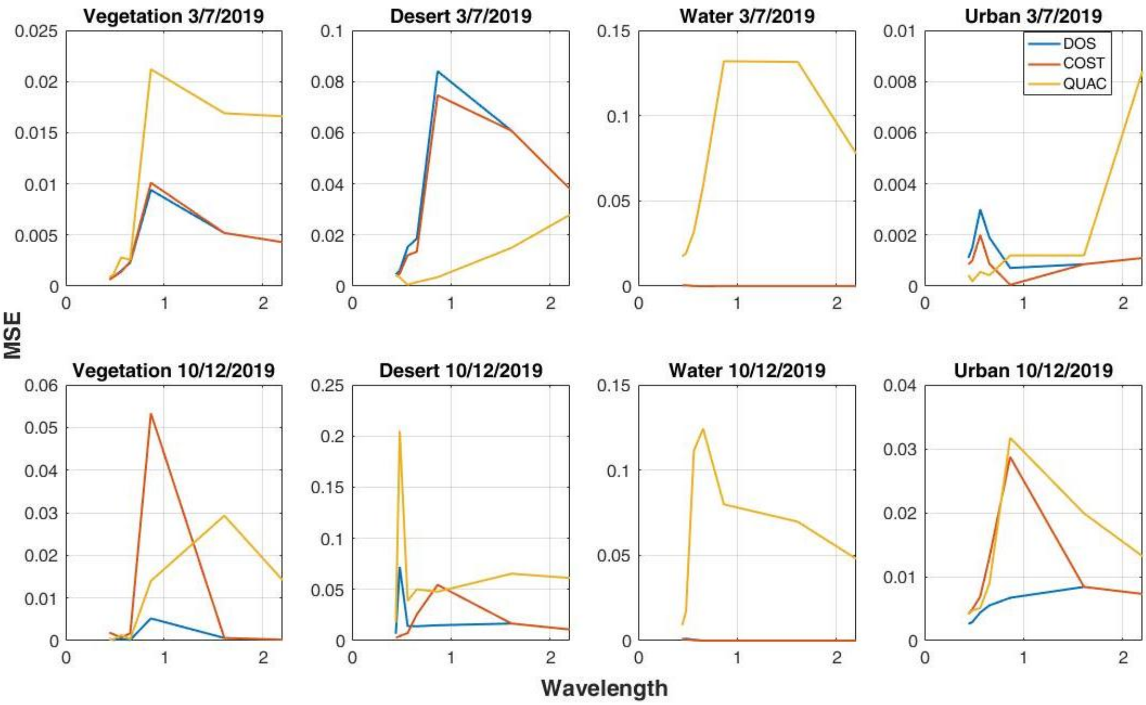

Fig. 3. the mean square error of the Landsat-8 compared to the Level 2A data

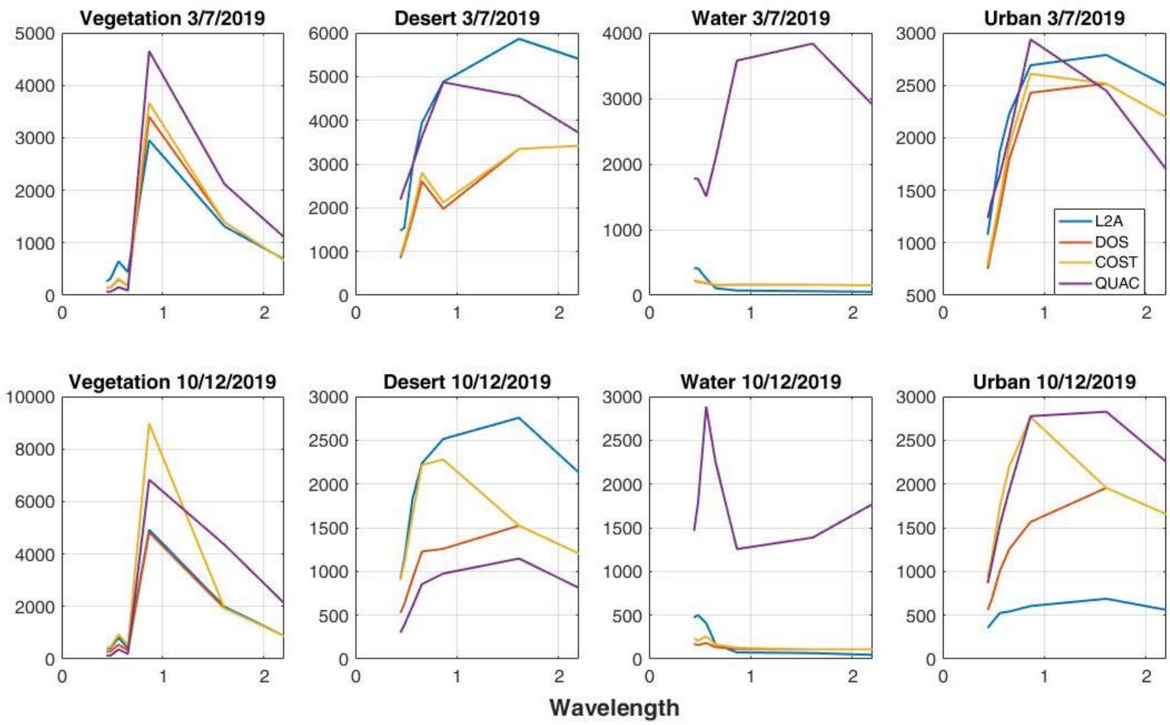

Fig. 4. The reflectance spectrum curve for the Landsat-8 data (Level 2A, DOS, COST, QUAC)

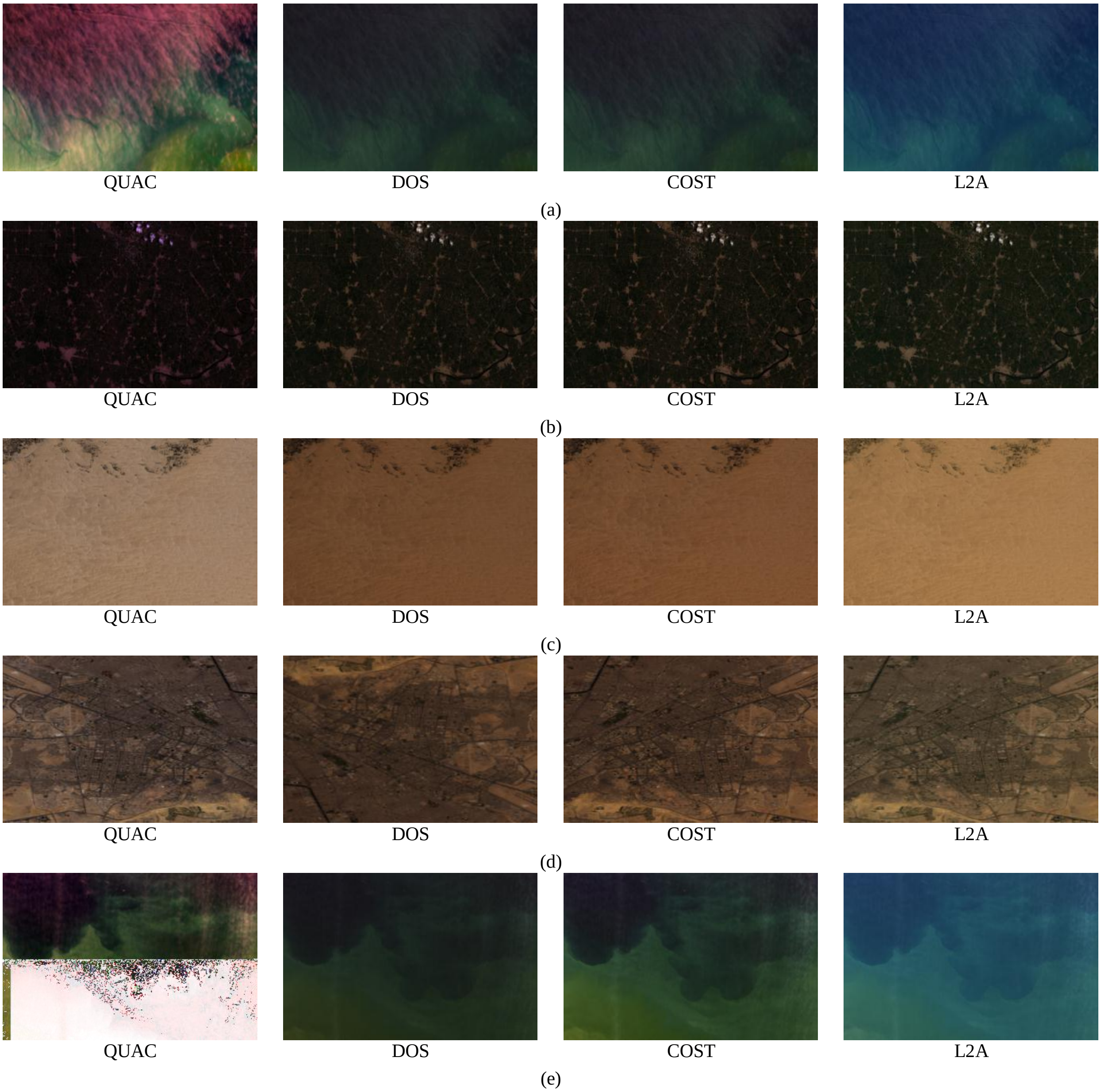
QUAC
DOS
COST
L2A
(a)
QUAC
DOS
COST
L2A
(b)
QUAC
DOS
COST
L2A
(c)
QUAC
DOS
COST
L2A
(d)
QUAC
DOS
COST
L2A
(e)

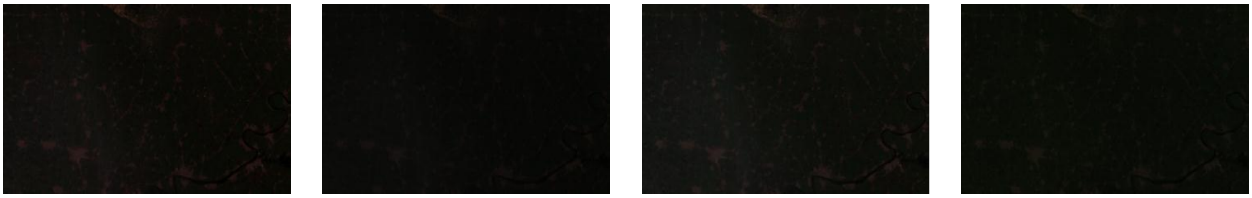

QUAC DOS COST L2A

(f)

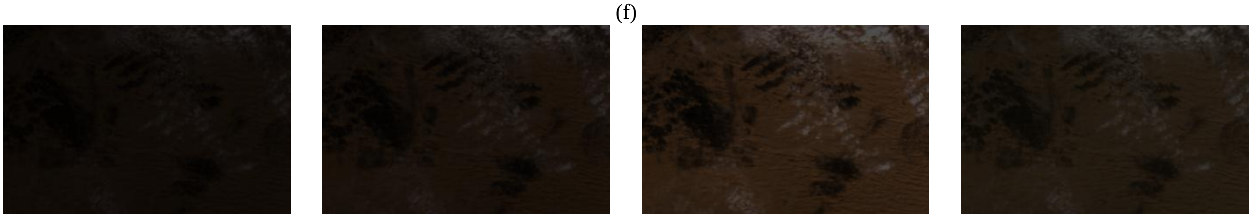

QUAC DOS COST L2A

(g)

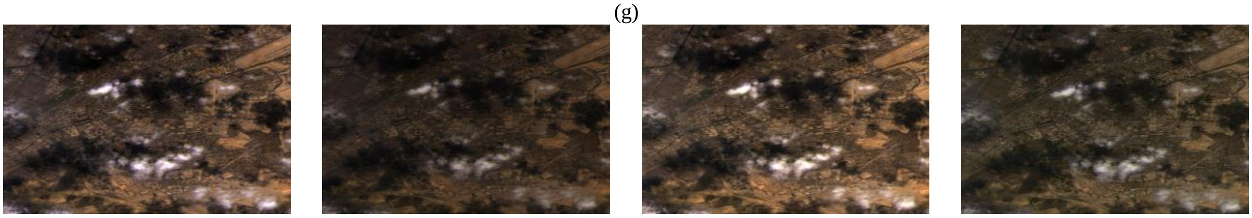

QUAC DOS COST L2A

(h)

Fig. 5. the resulted landsat-8 scene from DOS, COST, QUAC, Level 2A: ((a) Water scene, (b) Vegetation scene, (c) Desert scene, and (d) Urban scene in 3 July 2019) ; ((e) Water scene, (f) Vegetation scene, (g) Desert scene, and (h) Urban scene in 10 December 2019)

3.2. the Sentinel-2 results

Sentinel-2 results as might have been noted, the B10 is never computed because it lacks surface information and is only used to detect cirrus. From Figure 6 It's worth noting that the DOS result has a far higher error than Sen2Cor, but it's not more than 1% except in the desert scenes where the error exceeding 25% in the clear weather and 60% in the hazy weather. The lower error value for DOS is in the water scenes with error not exceeding 3*10-3 in clear weather and 8*10-3 in hazy weather. The Sentinel-2 findings, like the Landsat-8 results, show a peak at the NIR (B9) in most MSE graphs. This is because both vegetation and desert represent a large amount of energy in the NIR band, making the scene very bright and the dark target less, while water consumes a large amount of energy in the NIR band, making the scene much darker and therefore no beak in the MSE graph. From the spectrum curves Figure 7 it's clear that Sen2Cor is very close to the Level 2A where DOS go close to them in the vegetation scenes and the urban scene in clear weather while drifts so much far in the desert scene. In Figure 8 visual inspection reveals that DOS preserves image information and does not cause distortions, but it tends to overestimate the error.

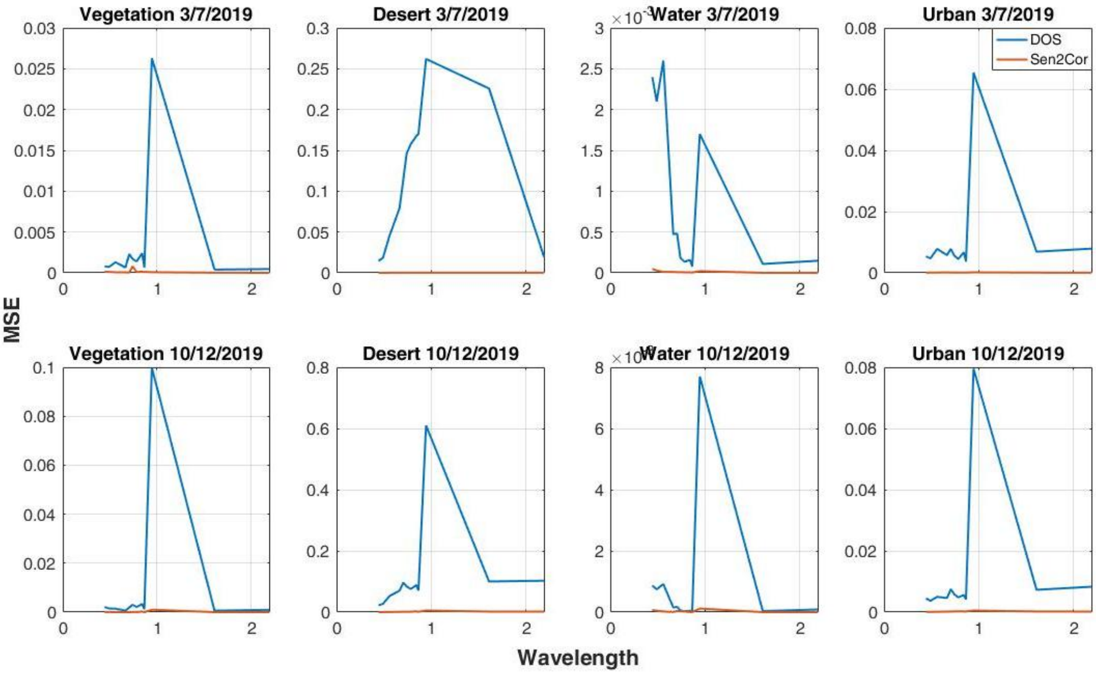

Fig 6: Mean square error of the Sentinel-2 compared to the Level 2A data

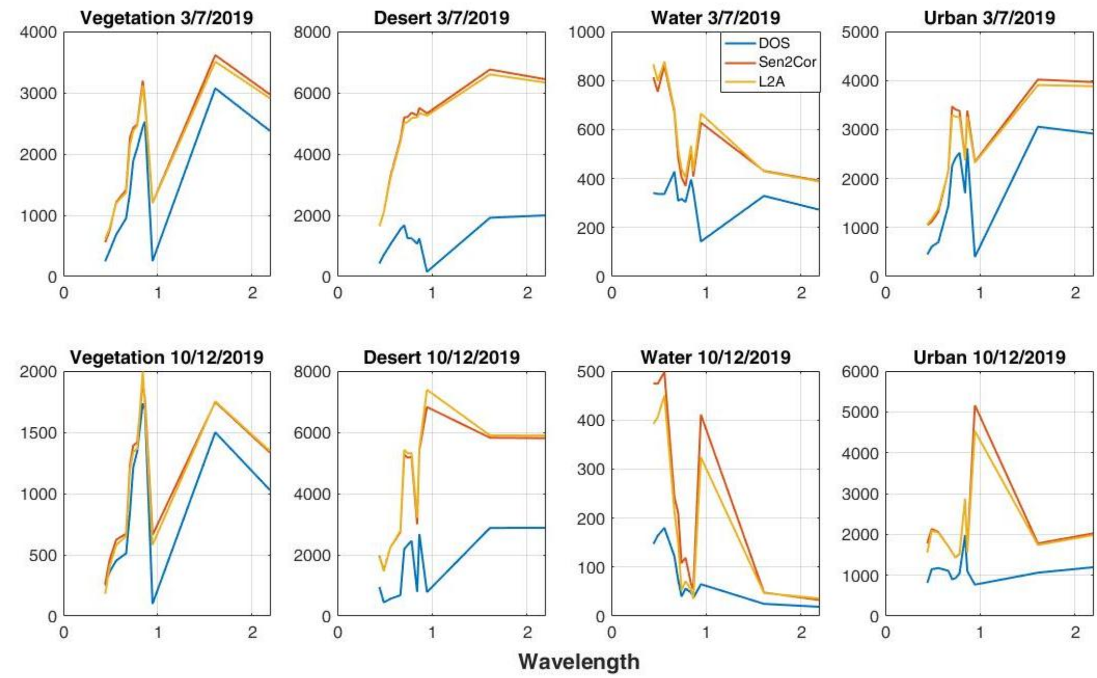

Fig 7: the reflectance spectrum curve for the Sentinel-2 data (DOS, Sen2Cor, Level 2A)

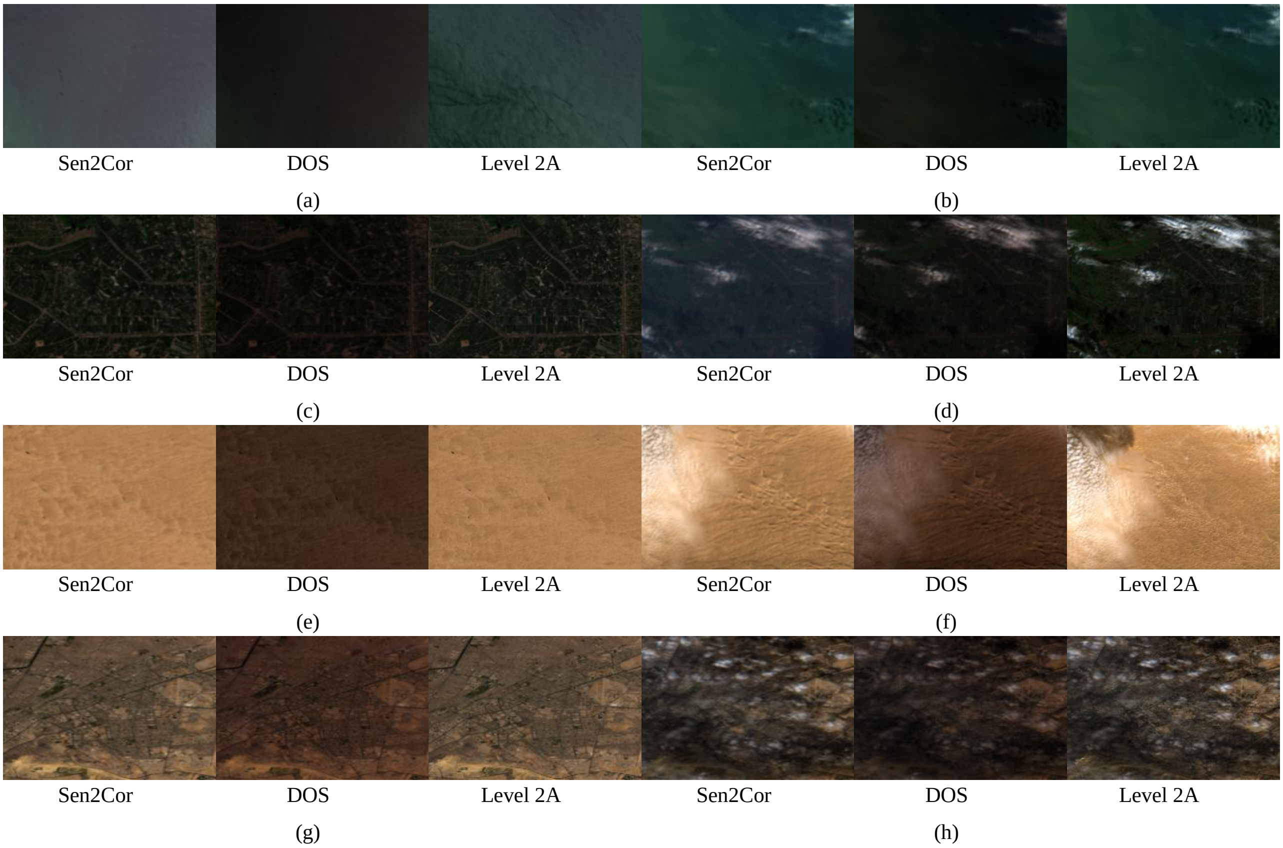

Fig. 8. Resulted Sentinel-2 scene from Sen2Cor, DOS, and Level 2A: ((a) Water scene, (b) Vegetation scene, (c) Desert scene, and (d) Urban scene in 3 July 2019); ((e) Water scene, (f) Vegetation scene, (g) Desert scene, and (h) Urban scene in 10 December 2019)

4. conclusion

This section demonstrates the effectiveness of the proposed workflow on Landsat-8 and Sentinel-2. The performance of the proposed atmospheric correction workflow was evaluated in terms overall accuracy (OA) which is the ratio of a sum of correctly identified pixels to the number of total pixels

, The images shown in Figure 5 and Figure 8 are true color images combined of the bands blue, green and red (band2, band 3 and band 4), respectively. The results are compared by calculating the mean square error MSE between the corrected image and the Level 2A image, comparing the spectrum curve of each scene and by visual inspection.

References

1. Hamimi, Z., Hagag, W., Kamh, S., and El-Araby, A., Application of remote-sensing techniques in geological and structural mapping of Atalla Shear Zone and Environs, Central Eastern Desert, Egypt. Arabian Journal of Geosciences, 2020. 13: p. 1-27.
2. Al-Nahmi, F., Saddiqi, O., Hilali, A., Rhinane, H., Baidder, L., and Khanbari, K., Application of remote sensing in geological mapping, case study Al Maghrabah area–Hajjah region, Yemen. ISPRS Annals of the Photogrammetry, Remote Sensing and Spatial Information Sciences, 2017. 4: p. 63-71.
3. Ahmad, H., Applications of remote sensing in oceanographic research. International Journal of Oceanography & Aquaculture, 2019. 3(1): p. 000159.
4. Weiss, M., Jacob, F., and Duveiller, G., Remote sensing for agricultural applications: A meta-review. Remote sensing of environment, 2020. 236: p. 111402.
5. Shanmugapriya, P., Rathika, S., Ramesh, T., and Janaki, P., Applications of remote sensing in agriculture-A Review. Int. J. Curr. Microbiol. Appl. Sci, 2019. 8(01): p. 2270-2283.
6. Sekertekin, A. and Arslan, N., Monitoring thermal anomaly and radiative heat flux using thermal infrared satellite imagery–A case study at Tuzla geothermal region. Geothermics, 2019. 78: p. 243-254.
7. Fuyi, T., Mohammed, S., Abdullah, K., Lim, H., and Ishola, K. A comparison of atmospheric correction techniques for environmental applications. in 2013 IEEE International Conference on Space Science and Communication (IconSpace). 2013. IEEE.
8. Spitzer, D., On applications of remote sensing for environmental monitoring. Environmental monitoring and assessment, 1986. 7: p. 263-271.

9. Joshi, A., Agrawal, S., and Chauhan, P., Reduction of atmospheric effects in satellite images during the COVID-19 induced lockdown. Journal of the Indian Society of Remote Sensing, 2020. 48: p. 1613-1625.
10. Solomon, S., Portmann, R., Sanders, R., and Daniel, J., Absorption of solar radiation by water vapor, oxygen, and related collision pairs in the Earth's atmosphere. Journal of Geophysical Research: Atmospheres, 1998. 103(D4): p. 3847-3858.
11. Arking, A., Absorption of solar energy in the atmosphere: Discrepancy between model and observations. Science, 1996. 273(5276): p. 779-782.
12. Fukushima, H., Higurashi, A., Mitomi, Y., Nakajima, T., Noguchi, T., Tanaka, T., and Toratani, M., Correction of atmospheric effect on ADEOS/OCTS ocean color data: Algorithm description and evaluation of its performance. Journal of Oceanography, 1998. 54: p. 417-430.
13. Frouin, R.J., Franz, B.A., Ibrahim, A., Knobelspiesse, K., Ahmad, Z., Cairns, B., Chowdhary, J., Dierssen, H.M., Tan, J., and Dubovik, O., Atmospheric correction of satellite ocean-color imagery during the PACE era. Frontiers in earth science, 2019. 7: p. 145.
14. Schott, J.R., Remote sensing: the image chain approach. 2007: Oxford University Press.
15. Van den Bosch, J. and Alley, R. Application of LOWTRAN 7 as an atmospheric correction to airborne visible/infrared imaging spectrometer (AVIRIS) data. in 10th Annual International Symposium on Geoscience and Remote Sensing. 1990. IEEE.
16. Wright, J., Evaluation of LOWTRAN and MODTRAN for use over high zenith angle/long path length viewing. 1991.
17. Berk, A., Bernstein, L.S., and Robertson, D.C., MODTRAN: A moderate resolution model for LOWTRAN 7. 1989, Geophysics Laboratory Hanscom AFB, MA, USA.
18. Vermote, E., Tanré, D., Deuzé, J., Herman, M., Morcrette, J., and Kotchenova, S., Second Simulation of a Satellite Signal in the Solar Spectrum-Vector (6SV), User Guide Version 3. Space Vehicles Directorate, Air Force Materiel Command, MA: Hanscom AFB: Air Force Research Laboratory, 2006.
19. Karpouzli, E. and Malthus, T., The empirical line method for the atmospheric correction of IKONOS imagery. International Journal of Remote Sensing, 2003. 24(5): p. 1143-1150.
20. Wu, J., Wang, D., and Bauer, M.E., Image-based atmospheric correction of QuickBird imagery of Minnesota cropland. Remote Sensing of Environment, 2005. 99(3): p. 315-325.
21. Nazeer, M., Nichol, J.E., and Yung, Y.-K., Evaluation of atmospheric correction models and Landsat surface reflectance product in an urban coastal environment. International journal of remote sensing, 2014. 35(16): p. 6271-6291.
22. Chavez Jr, P.S., An improved dark-object subtraction technique for atmospheric scattering correction of multispectral data. Remote sensing of environment, 1988. 24(3): p. 459-479.
23. Moran, M.S., Jackson, R.D., Slater, P.N., and Teillet, P.M., Evaluation of simplified procedures for retrieval of land surface reflectance factors from satellite sensor output. Remote Sensing of Environment, 1992. 41(2-3): p. 169-184.
24. Chavez, P.S., Image-based atmospheric corrections-revisited and improved. Photogrammetric engineering and remote sensing, 1996. 62(9): p. 1025-1035.
25. Jorge, D.S.F., Amore, D., and Barbossa, C., Efficiency estimation of four different atmospheric correction algorithms in a sediment-loaded tropic lake for Landsat 8 OLI sensor. Proceedings of the Anais XVII Simpósio Brasileiro de Sensoriamento Remoto—SBSR, João Pessoa-PB, Brasil, 2015: p. 25-29.
26. Dewi, E.K. and Trisakti, B., Comparing atmospheric correction methods for Landsat OLI data. International Journal of Remote Sensing and Earth Sciences (IJReSES), 2017. 13(2): p. 105-120.
27. Shi, L., Mao, Z., Chen, P., Gong, F., and Zhu, Q. Comparison and evaluation of atmospheric correction algorithms of QUAC, DOS, and FLAASH for HICO hyperspectral imagery. in Remote Sensing of the Ocean, Sea Ice, Coastal Waters, and Large Water Regions 2016. 2016. SPIE.
28. Lantzanakis, G., Mitraka, Z., and Chrysoulakis, N. Comparison of physically and image based atmospheric correction methods for Sentinel-2 satellite imagery. in Perspectives on atmospheric sciences. 2017. Springer.
29. Wicaksono, P. and Hafizt, M., Dark target effectiveness for dark- object subtraction atmospheric correction method on mangrove above- ground carbon stock mapping. IET Image Processing, 2018. 12(4): p. 582-587.
30. Wang, Z., Xia, J., Wang, L., Mao, Z., Zeng, Q., Tian, L., and Shi, L., Atmospheric correction methods for GF-1 WFV1 data in hazy weather. Journal of the Indian Society of Remote Sensing, 2018. 46: p. 355-366.
31. Rumora, L., Miler, M., and Medak, D., Contemporary comparative assessment of atmospheric correction influence on radiometric indices between Sentinel-2A and Landsat 8 imagery. Geocarto International, 2021. 36(1): p. 13-27.
32. Lhissou, R., El Harti, A., Maimouni, S., and Adiri, Z., Assessment of the image-based atmospheric correction of multispectral satellite images for geological mapping in arid and semi-arid regions. Remote Sensing Applications: Society and Environment, 2020. 20: p. 100420.
33. Muchsin, F., Pradono, K.A., Prasasti, I., Dianovita, D., Ulfa, K., Veronica, K.W., Novresiandi, D.A., and Ibrahim, A., EFFECT OF ATMOSPHERIC CORRECTION ALGORITHM ON LANDSAT-8 AND SENTINEL-2 CLASSIFICATION ACCURACY IN PADDY FIELD AREA. International Journal of Remote Sensing and Earth Sciences (IJReSES), 2023. 20(1): p. 57-65.
34. Bernstein, L.S., Jin, X., Gregor, B., and Adler-Golden, S.M., Quick atmospheric correction code: algorithm description and recent upgrades. Optical engineering, 2012. 51(11): p. 111719-111719.
35. Bernstein, L.S., Adler-Golden, S.M., Sundberg, R.L., Levine, R.Y., Perkins, T.C., Berk, A., Ratkowski, A.J., Felde, G.W., and Hoke, M.L. A new method for atmospheric correction and aerosol optical property retrieval for VIS-SWIR multi- and hyperspectral imaging sensors: QUAC (QUick Atmospheric Correction). in INTERNATIONAL GEOSCIENCE AND REMOTE SENSING SYMPOSIUM. 2005.
36. Mondejar, J.P. and Tongco, A.F., Near infrared band of Landsat 8 as water index: a case study around Cordova and Lapu-Lapu City, Cebu, Philippines. Sustainable Environment Research, 2019. 29: p. 1-15.
37. Segl, K., Richter, R., Küster, T., and Kaufmann, H., End-to-end sensor simulation for spectral band selection and optimization with application to the Sentinel-2 mission. Applied Optics, 2012. 51(4): p. 439-449.
38. Gatti, A. and Bertolini, A., Sentinel-2 products specification document. Rapport technique, 2015: p. 4-7.
39. Warren, M.A., Simis, S.G., Martinez-Vicente, V., Poser, K., Bresciani, M., Alikas, K., Spyrakos, E., Giardino, C., and Ansper, A., Assessment of atmospheric correction algorithms for the Sentinel-2A MultiSpectral Imager over coastal and inland waters. Remote sensing of environment, 2019. 225: p. 267-289.
40. Main-Knorn, M., Pflug, B., Louis, J., Debaecker, V., Müller-Wilm, U., and Gascon, F. Sen2Cor for sentinel-2. in Image and signal processing for remote sensing XXIII. 2017. SPIE.